# Journal of Materials Chemistry A

Accepted Manuscript


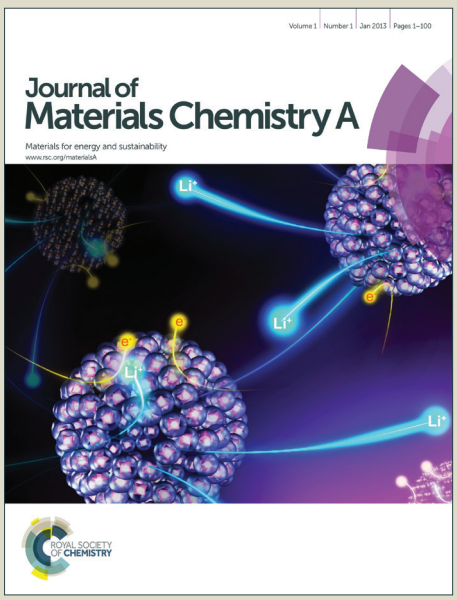





ROYAL SOCIETY OF CHEMISTRY

www.rsc.org/materialsA

Cite this: DOI: 10.1039/c0xx00000x

www.rsc.org/xxxxxx

ARTICLE TYPE

# Superior Sodium Intercalation of Honeycomb-structured Hierarchical Porous $Na_3V_2(PO_4)_3$/C Microball Prepared by a Facile One-pot Synthesis

**Qiuyue Wang[a,‡], Baidan Zhao[a,‡], Sen Zhang*[,b], Xiaohui Gao[c], Chao Deng*[,a]**

***Received (in XXX, XXX) Xth XXXXXXXXX 20XX, Accepted Xth XXXXXXXXX 20XX***
**DOI: 10.1039/b000000x**

Tailoring materials into hierarchical porous micro/nanostructure offers unprecedented opportunities in the utilization of their functional properties. Particularly, it is crucial for the electrode materials to realize high-performance because of the advantages such as large surface area, superior structure stability and short ion transport pathway. Here we report the design of a new architecture, named "honeycomb-type hierarchical porous microball", for $Na_3V_2(PO_4)_3$ by a facile one-pot synthesis. The network between nanovoids is formed by *in-situ* carbonization of surfactants (CTAB) along with the crystallization of $Na_3V_2(PO_4)_3$, which results in the hierarchical porous $Na_3V_2(PO_4)_3$ skeleton with surface conductive layer. The prepared $Na_3V_2(PO_4)_3$/C composite consists of spherical particle filled with hierarchical pores and interconnective nanochannels, resulting in the honeycomb-type architecture. It not only enables easier electrolyte penetration, but also provides high-efficient electron/ion transport pathway for fast sodium intercalation. Both the GITT and EIS results demonstrate the improved sodium diffusion capability and decreased electrochemical resistance for the honeycomb-structured microball in comparison to the microsized nonporous reference samples. Moreover, it also delivers superior high rate capability and cycling stability, which retains 93.6% of the initial capacity after 200 cycles at the 1 *C* rate. Even at 20 *C*, it still delivers a high capacity of 80.2 $mAh \cdot g^{-1}$ corresponding to 71% of the capacity. Given the superior ion intercalation kinetics and excellent structure stability, the honeycomb-type structure puts forward a new strategy to develop high-performance polyanion-based materials for low-cost and high-power "rocking-chair" batteries.

KEYWORDS: honeycomb-type structure; hierarchical porous microball; electrode material; sodium intercalation chemistry

## 1 Introduction

With the rapid development of portable electronic devices and hybrid electric vehicles, rechargeable batteries with high storage capacity and cycling stability become the versatile, clean and promising energy storage systems[1]. Among the rechargeable batteries, lithium ion battery with the highest energy density is a prime candidate. However, the disadvantages such as high cost and scarce resource of lithium limit its application[2-5]. Therefore, the employment of other guest ions as alternatives to lithium ion is favorable to further development of low-cost power sources. The abundant resource and low cost of sodium make sodium-ion battery a promising alternative to lithium-ion batteries[6-8]. However, the larger ionic radius of $Na^+$ than that of $Li^+$ leads to its poor kinetic and inferior rate capability[9]. Therefore, it is still a big challenge to discover new sodium intercalation hosts with fast ion intercalation capability.

Many approaches have been proposed on the electrode materials to improve their ion transport kinetics, such as fabricating novel structures to control particle size and morphology[10,11], cations doping[12,13] and building surface conductive layer[14,15]. Among all these strategies, three-dimensional hierarchical porous (3DHP) structure with short ion diffusion distance, as well as enlarged electrode/electrolyte interfacial area, has demonstrated the superiority in energy storage applications[16-27]. It possesses a lot of interconnective pores inside the particles, which facilitates the uniform distribution of electrolyte and allows a high efficient mass transport between the electrolyte and electrode. Moreover, the hierarchical pores also act as a buffer layer that alleviates volume change during ion insertion/extraction, which is favorable to structure stability and cycling stability. Inspired by these advantages, many metal oxides such as NiO[16], $MoO_x$[17], $TiO_2$[18], $V_2O_5$[19,20], MnO[21] and simple inorganic materials such as C[22-24], Si[25], Ni[26] and so on, with 3DHP structure have been synthesized and applied in electrochemical systems. However, the construction of 3DHP structure for more complex materials, such as polyanion-based materials, is rarely reported and remains largely unexplored[27]. Thus it is challenging to construct this high-efficient architecture for polyanion-based electrode materials to achieve superior electrochemical properties. Particularly, it is

especially urgent for the polyanions in sodium ion batteries, which have intrinsically poorer kinetic and inferior rate capability than those in lithium system[6-9].

Following this viewpoint, for the first time, we report the design of a new structure, named "honeycomb-type hierarchical porous microball" for the polyanion-based electrode material in sodium ion battery. We choose $Na_3V_2(PO_4)_3$ as a model material, and this strategy can also be applied to other polyanions as well. With the NASCION (Na super-ionic conductor) structure, $Na_3V_2(PO_4)_3$ has high capacity, good thermal stability and large interstitial channels, which make it a good candidate for sodium de/intercalation[28-32]. In this study, the honeycomb-structured $Na_3V_2(PO_4)_3$/C is fabricated by a simple one-pot synthesis. The cetyltrimethylammonium bromide (CTAB) is employed simultaneously as carbon source and soft template to construct the hierarchical porous architecture. As illustrated in Figure 1, the prepared $Na_3V_2(PO_4)_3$/C composite exhibits spherical particle filled with macro/mesopores and interconnective nanochannels, which facilitates electrolyte penetration and promotes high-efficient ion transport. Moreover, the network between the nanovoids is coated by *in-situ* carbon. It also provides continuous electron pathways for fast electron transfer. Both advantages on electron and ion transport are favorable to enhancing the kinetics of $Na_3V_2(PO_4)_3$/C composite. Furthermore, the outside spherical morphology makes up the insufficient volume energy density of porous material, which offsets the fatal defect of porous architecture in electrochemical systems.

Inspired by these advantages, the sodium ion chemistry of honeycomb-structured $Na_3V_2(PO_4)_3$/C microball is carefully evaluated. As evidenced by GITT, EIS and galvanostatic charge/discharge results, the honeycomb-structured composite exhibits improved sodium diffusion capability, superior high rate property and good cycling stability. The results demonstrate the high efficiency and significant potential of honeycomb-type architecture in the polyanion-based materials for "rocking-chair" batteries.

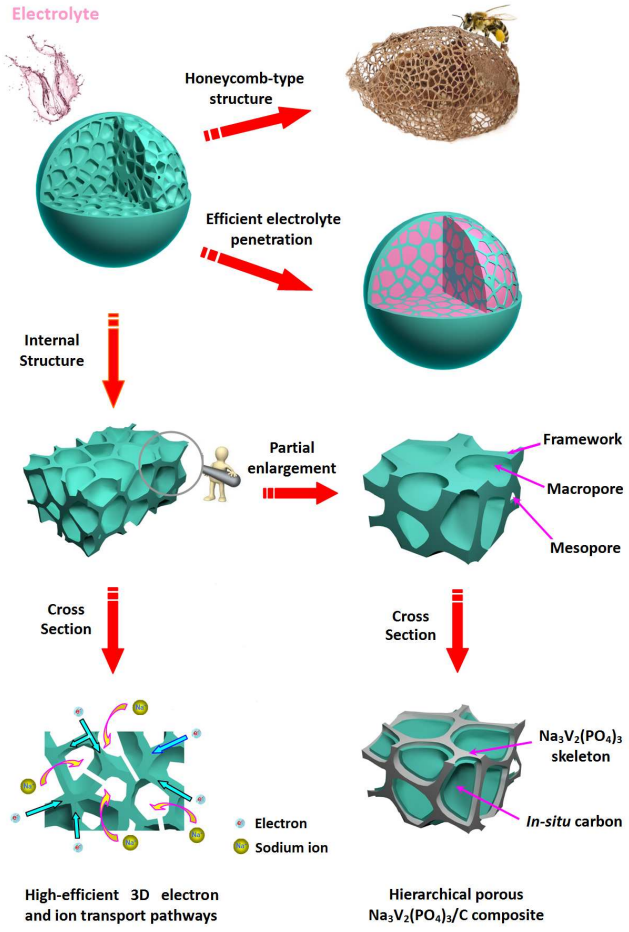


Figure 1 Scheme of honeycomb-type structured $Na_3V_2(PO_4)_3$/C microball with spherical particle and hierarchical porous architecture. The partial enlarged image emphasizes the bulk $Na_3V_2(PO_4)_3$ skeleton and surface *in-situ* carbon layer. The cross section image with high-efficient electron/ion transport pathways is illustrated.

## 2 Experimental

*2.1 Synthesis.*

All the reagents were used without further purifying. The honeycomb-structured $Na_3V_2(PO_4)_3$/C microball was prepared by a facile one-pot synthesis. The starting materials are $V_2O_5$, $Na_2CO_3$, $NH_4H_2PO_4$, oxalic acid and cetyltrimethylammoniumbromide (CTAB). Firstly, stoichiometric amount of $V_2O_5$ was dissolved into $H_2O_2$ (30%) solution under vigorously stirring for three days until a clear sol was formed. Then it was transferred to a water bath at 80 $^oC$ and continuously stirring for half an hour. The oxalic acid was mixed into the solution, followed by the mixture of $Na_2CO_3$ and $NH_4H_2PO_4$. Finally, the CTAB was dissolved in 20 ml deionic water, which was slowly added into the resultant solution dropwise. The mixture kept stirring at 80 $^oC$ until it turns to a blue sol. After dying the dying the gel in an oven, the precursor was grounded in a motor. Finally, the result precursor was annealed at 700 $^oC$ for 7 hours in an argon atmosphere to achieve the final product.

For comparison, the reference sample with nonporous architecture, microsized particles and low carbon content is prepared by conventional solid-state approach. Stoichiometric amounts of $V_2O_5$, $Na_2CO_3$, $NH_4H_2PO_4$ and glucose were dispersed in alcohol and then ball milled by a planetary high-energy ball mill at a rotation speed of 400 rpm for 10 hours. After the evaporation of alcohol, the solid mixture was sintered at 400 $^oC$ for 4 hours in argon atmosphere. The obtained powder was regrounded and sintered at 800 $^oC$ for 12 hours in an argon atmosphere.

The obtained reference material with low carbon content is mixed with sucrose and then sintered at 800 $^oC$ for 2 hours in an argon atmosphere. The product with surface carbon layer and microsized particles is described as carbon-coated reference sample.

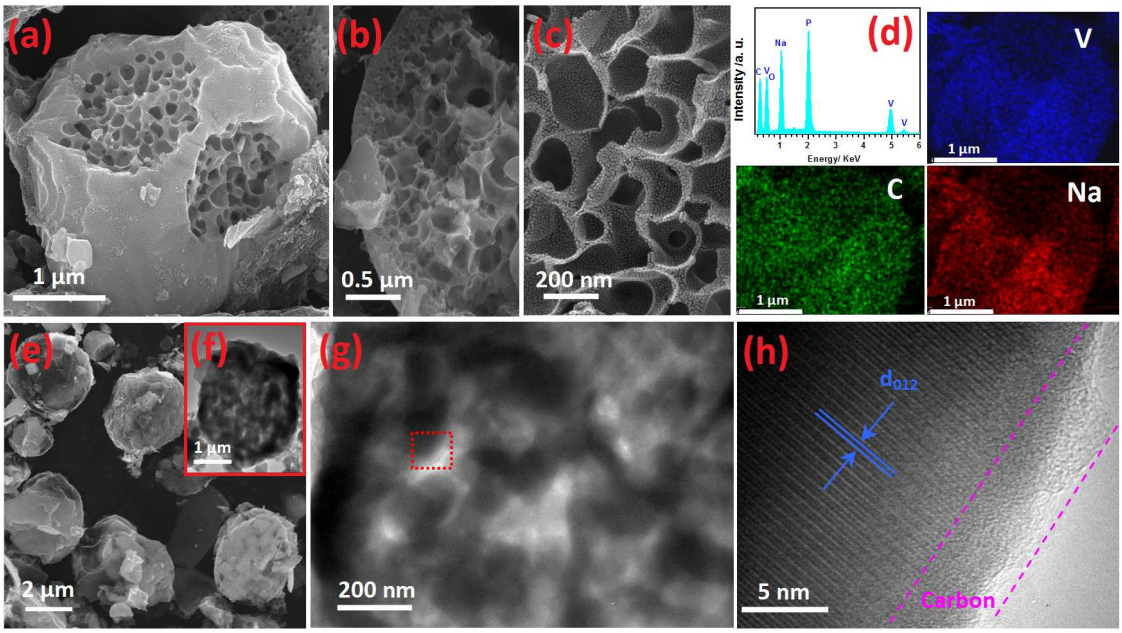


Figure 2 Morphologies of the honeycomb-structured $Na_3V_2(PO_4)_3$/C microball: (a) SEM image of the microball filled with hierarchical pores, (b) SEM image of its cross-section and (c) enlarged image of hierarchical pores, (d) EDX spectroscopy and elements (C, Na, V) mapping images, (e) low resolution SEM image of the $Na_3V_2(PO_4)_3$ microballs, (f) TEM image of the hierarchical porous microball and (g) its partial enlarged image, (h) HRTEM image of the framework in the porous microball as emphasized in the red square of g.

*2.2 Materials characterization*

Powder X-ray diffraction (XRD, Bruker D8/Germany) using Cu Kα radiation was employed to identify the crystalline phase of the material. The experiment was performed by using step mode with a fixed time of 3 s and a step size of 0.02°. The XRD pattern was refined by using the Rietveld method. The morphology was observed with a scanning electron microscope (SEM, HITACHIS-4700) and a transmission electron microscope (TEM, JEOS-2010 PHILIPS). Nitrogen adsorption-desorption isotherms were measured using a Micromeritics ASAP 2010 sorptometer and specific surface area and pore size distribution were calculated correspondingly. Carbon contents of the samples were determined by an element analyzer (EA, Elementar Vario EL).

*2.3 Electrochemical measurements*

The electrochemical characteristics were measured in CR2032 coin cells. The coin cells were assembled in an argon filled glove box. Each composite electrode was made from a mixture of the active material, carbon black and polyvinylidene fluoride (PVDF) in a weight ratio of 8:1:1. Na foil was employed as counter and reference electrode and 1 $mol \cdot L^{-1}$ $NaClO_4$ dissolved in propylene carbonate (PC) was used as electrolyte. For the galvanostatic intermittent titration technique (GITT), a constant current of 0.05 C was applied for 10 min and then interrupted to open circuit condition for 60 min. This process was repeated until the cathode potential exceeded the cut-off potential. Galvanostatic charge-discharge tests were performed in the potential range of 2.5~3.8 V vs. $Na/Na^+$ at ambient temperature on a Land battery testing system (Wuhan, China). EIS measurements were conducted at a fully discharged state using a Zivelab electrochemical workstation, and the applied frequency range is 100k~0.05 Hz.

## 3 Results and Discussion

The morphology of honeycomb-structured sample is characterized by SEM and TEM observations. Based on the SEM observation (Figure 2a), the composite has spherical particle with the diameter of ~3 μm. The cross-section image (Figure 2b) indicates the existence of macropores with the size of 100~200 nm inside the microballs. Moreover, the voids in the wall of the macropores provides interconnection between the macropores, which results in smaller mesopores with the size of 5~30 nm (Figure 2c). The uniformity of the material is evidenced by low-magnification SEM image in Figure 2e. A more complete understanding of structure inside the microball is provided by TEM observation. As displayed in Figure 2(f, g), both sized macro/micropores uniformly distribute inside the spherical particle. They construct the hierarchical porous architecture and result in the honeycomb-like structure for the composite. The voids on the network between hierarchical pores build connective nanochannels inside the particle, which facilitates electrolyte penetration and promotes ion transport. The detailed structure of network inside the microball is further indentified by high-resolution TEM (HRTEM). A shown in Figure 2(h), the network is composed of the bulk skeleton and the surface layer. The well-resolved lattice fringe with an interplanar distance of 0.62 nm corresponds to the (012) lattice planes of the $Na_3V_2(PO_4)_3$, which confirms the single crystal nature of the skeleton. The surface nanolayer arising from residual carbon has the thickness of 2~3

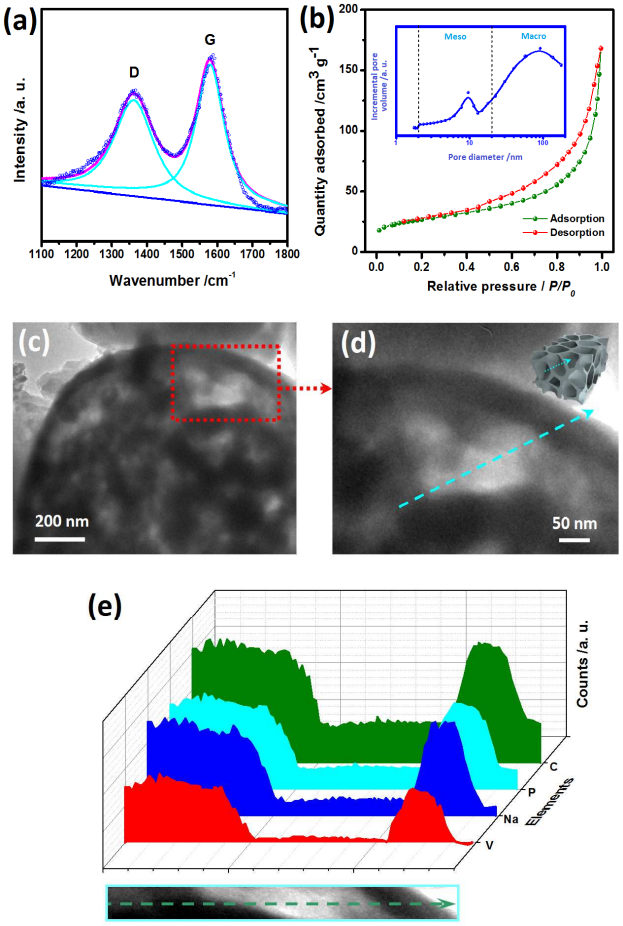


Figure 3 (a) Raman and (b) Nitrogen sorption isotherms of the honeycomb-structured $Na_3V_2(PO_4)_3$/C microball. The pore size distribution is displayed as inset of (b). TEM images of the whole honeycomb-structure (c) and partial enlarged image (d). The schematic image is shown as inset of (d). (e) Corresponding line-scan TEM-EDS element analysis results.

nm, which constructs the 3D conductive framework and provides continuous electron transport pathways inside the microball. Moreover, the EDX spectroscopy and element mapping image (Figure 2d) also certify the existence and uniform distribution of C, Na, V, P elements, which coincides with the TEM results. Therefore, the results demonstrate that the honeycomb-structured hierarchical porous microballs have been successfully constructed, which have high-efficient electron/ion pathways and are favorable to fast ion intercalation chemistry.

Raman spectroscopy is recorded to further characterize the nature of carbon in the honeycomb-structured $Na_3V_2(PO_4)_3$/C microball. Two characteristic signatures located at ~1360 and 1582 $cm^{-1}$ are observed for the composite (Figure 3a), corresponding to the *D* (disordered carbon) and *G* (graphene carbon) bands[33,34]. The low value of the *D*/*G* intensity ratio (0.99) indicates the higher amount of $sp^2$-type carbon than the $sp^3$-type one. It demonstrates that the *in-situ* carbon on the surface of $Na_3V_2(PO_4)_3$ skeleton is partially graphitized. It is favorable to enhancing the electrical conductivity and facilitates fast electron transport.

Nitrogen sorption isotherms are generated to investigate the Brunauer-Emmet-Teller (BET) surface and the porous structure of the sample. As displayed in Figure 3(b), significant hysteresis loop indicates the high porous structure of the composite. The composite possesses a high specific surface area of 87.3 $m^2$ $g^{-1}$ and large pore volume of 0.38 $cm^3$ $g^{-1}$. The steep increase of absorption curve at high pressure ($P/P_0$=0.8~0.99) indicates the pore volume is not only produced by mesopores, but also by macropores with a larger size[35]. A detailed statistics on the pore size distribution is employed. As displayed in inset of Figure 3(b), bimodal porosity presents in the composite: ~10 nm mesopores (2-50 nm) and ~96 nm macropores (>50 nm). The results certify the hierarchical porous architecture of the honeycomb-structured composite. The generation of mesopores is associated with the open voids on the walls of the macropores inside the microball, which is coincided with above SEM and TEM results. To further verify the hierarchical porous architecture, the line-scan element analysis is carried out on the cross section of a selected void (Figure 3c,d). Combined the intensity profiles of elements along with the straight line, each element signal exhibits similar tendency (Figure 3e). It demonstrates the hollow nature in the void. Such porous structure not only provides good contact between the electrolyte and active material, but also promotes high-efficient ion transport. Both advantages result in the enhanced ion intercalation chemistry and improved reversible electrochemical property for the honeycomb-structured microball.

The crystal structure of honeycomb-structured $Na_3V_2(PO_4)_3$/C microball is identified by X-ray diffraction (XRD). In order to clarify the advantage of honeycomb structure, two reference samples, *i.e.* the low carbon-content reference sample and carbon-coated reference sample, are employed in this study. The physical characteristics of all three materials are displayed in Table 1. The values of pore volume and specific surface area for the low carbon-content sample are extremely low, which is associated with its microsized particle and solid morphology (Figure S1 a and b). A surface layer is observed on the carbon-coated reference sample, which results in the increased specific surface and pore volume (Figure S1 c and d). However, these improvements are not remarkable for the carbon-coated reference sample because it remains large microsized particles with solid morphology. On the other hand, the honeycomb-structured material displays much higher surface area and pore volume than both reference samples, indicating the dominant role of hierarchical pores in the physical characteristics of honeycomb-type structure.

XRD patterns of all the samples are displayed in Figure 4 (a). The diffraction peaks of all the samples can be readily indexed to the NASICON structure with $R\bar{3}c$ space group (rhombohedral, no. 167) without any impurity phases. The carbon-coated reference sample exhibits slightly decreased peak intensities than the low carbon-content reference sample. But

Table 1 Comparison of the BET area, pore volume and carbon content of (a) honeycomb-structured microball, (b) low carbon-content reference sample and (c) carbon coated reference sample.

| Materials | BET area /$m^2g^{-1}$ | Pore volume/$m^3g^{-1}$ | Carbon content/wt.% |
|---|---|---|---|
| a | 87.3 | 0.380 | 4.031 |
| b | 4.05 | 0.018 | 0.596 |
| c | 19.6 | 0.109 | 3.782 |

both references samples exhibit much higher peak intensities than the honeycomb-structured sample. The lower crystallinity of the honeycomb-structured sample is attributed to its high-porous structure and small crystals inside the microball. Rietveld refinement is carried out to more preciously estimate the $Na_3V_2(PO_4)_3$ phase. As displayed in Figure 4(b), the calculated pattern matches well with the observed one, certifying the reliability of the calculations. The atomic parameters obtained by Rietveld refinement of all the samples are summarized in Table 2, S1 and S2. The atomic parameters and lattice parameters of all three samples are coincided with previous literatures[28-32].

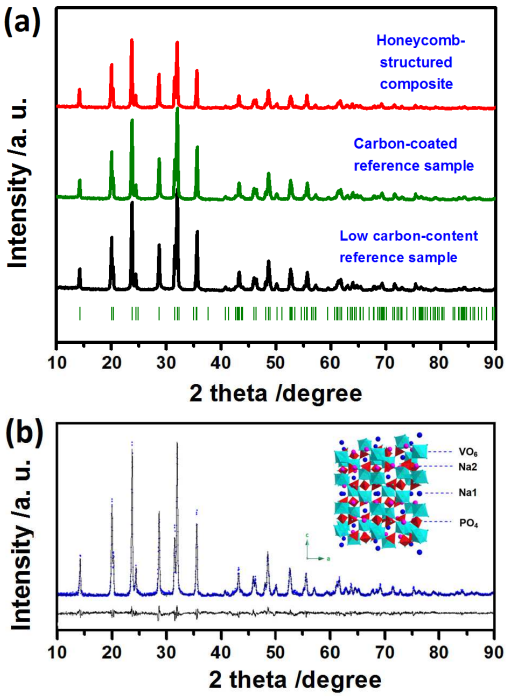


Figure 4 (a) Comparison of XRD patterns between the honeycomb-structured $Na_3V_2(PO_4)_3$/C microball, carbon-coated reference and low carbon-content reference sample. (b) Rietveld result of the honeycomb-structured microball and the crystal structure of $Na_3V_2(PO_4)_3$ is illustrated as inset. Units of $VO_6$, $PO_4$ and cations Na1, Na2 are indicated by different colors.

The crystal structure of $Na_3V_2(PO_4)_3$ is illustrated in inset of Figure 4(b). Two $VO_6$ octahedron connects three $PO_4$ tetrahedra via corners sharing, which constructs the basic unit of three-dimensional $[V_2(PO_4)_3]$ framework. Sodium ions are located in the voids of the framework with two different oxygen environments: one occupies the 6*b* site (Na1) and the other occupies the *18e* site (Na2). The 3D framework of $Na_3V_2(PO_4)_3$ not only provides large interstitial spaces for sodium accommodation, but also offers open channels for ion transport. Therefore, $Na_3V_2(PO_4)_3$ is considered to be a good candidate in sodium ion hosts. Combined above results, it confirms that the $Na_3V_2(PO_4)_3$/C composite with desirable single-phase structure and honeycomb-type morphology has been synthesized in this work.

Table 2 Atomic parameters of honeycomb-structured $Na_3V_2(PO_4)_3$/C material refined from the XRD data. ($a$=8.7327(7) Å, $c$=21.8248(3) Å)

| Atom | Wyckoff site | *x* | *y* | *z* |
|---|---|---|---|---|
| Na1 | 6b | 0 | 0 | 0 |
| Na2 | 18e | 0.6424 | 0 | 1/4 |
| V | 12c | 0 | 0 | 0.1479 |
| P | 18e | 0.2866 | 0 | 1/4 |
| O1 | 36f | 0.1763 | 0.9591 | 0.1923 |
| O2 | 36f | 0.1909 | 0.1585 | 0.0876 |

The sodium ion intercalation chemistry of the honeycomb-microball, carbon-coated reference and low carbon-content reference materials are investigated. GITT and EIS techniques are employed to evaluate their sodium diffusion capability. Figure 5(a) displays the GITT curves and corresponding quasi open-circuit potential (QOCP) during discharge process. For all the samples, the QOCP curves have one discharge plateau (at ~3.4 V) induced by the redox reaction of the $V^{3+}/V^{4+}$ couple, which is coincided with the two-phase reaction mechanism of $Na_3V_2(PO_4)_3$[28-30]. The apparent sodium diffusion coefficients of both samples can be calculated based on the GITT curves[36]. According to the Fick's second law of diffusion, $D_{Na}$ can be calculated from the following equation:

$$D_{Na} = \frac{4}{\pi}\left(\frac{m_B V_m}{M_B A}\right)^2 \left(\frac{\Delta E_S}{\tau\left(\frac{dE_\tau}{d\sqrt{\tau}}\right)}\right)^2 \quad (\tau \ll L^2/D_{Na}) \qquad (1)$$

where $D_{Na}$ ($cm^2s^{-1}$) is the sodium diffusion coefficient; $m_B$, $M_B$ and $V_m$ are the mass, molecular weight and molar volume of the electrode material, respectively; A is the interfacial area between electrode and electrolyte; $\tau$ is duration of the current pulse. If the relationship between $E$ and $\tau^{1/2}$ is linear, the equation (1) can be simplified as following:

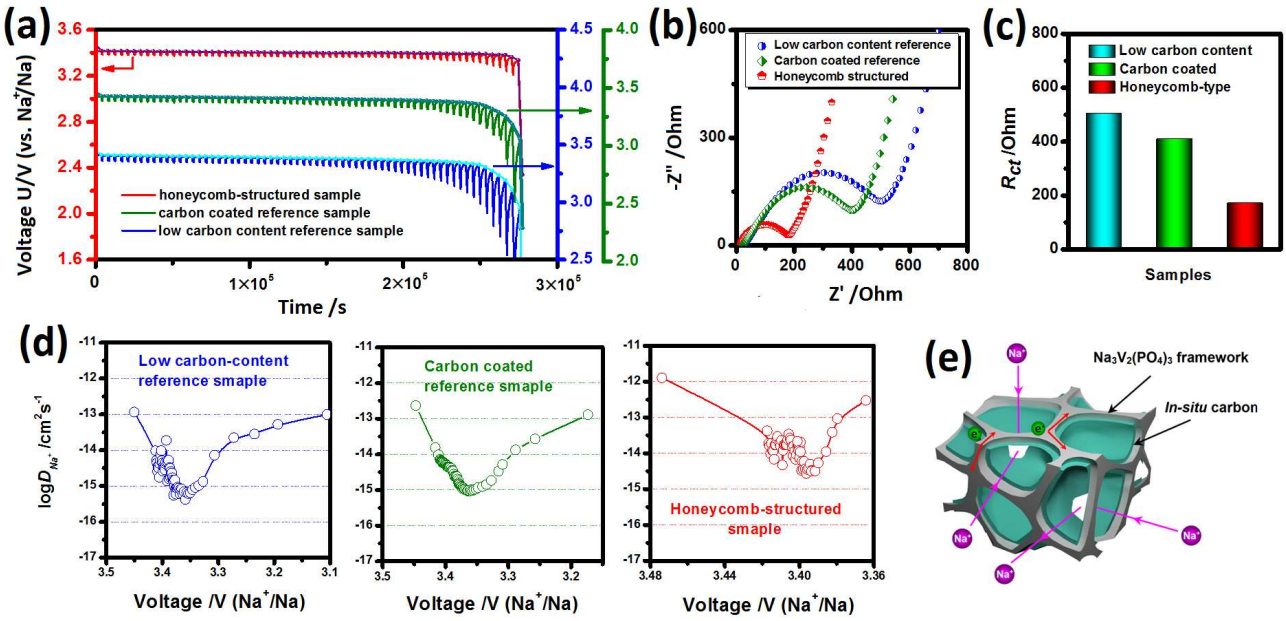


Figure 5 (a) GITT curves and corresponding QOCP curves for the honeycomb-structured microball, carbon-coated reference and low carbon-content reference samples. (d) The calculated sodium diffusion coefficients ($D_{Na}$) of all the samples based on GITT evaluations. (b) Nyquist plots and (c) corresponding charge transfer resistances ($R_{ct}$) of all the samples. (f) Schematic image of high-efficient electron/ion transport pathways in the honeycomb-type architecture is also illustrated.

$$D_{Na} = \frac{4}{\pi\tau}\left(\frac{m_B V_m}{M_B A}\right)^2\left(\frac{\Delta E_S}{\Delta E_\tau}\right)^2 \qquad (2)$$

The linear relationship between $E$ and $\tau^{1/2}$ (Figure S2) validates the applicability of the equation (2) in this study. Figure 5(d) shows the variation of $D_{Na}$ as a function of voltage for all the samples. All of the samples exhibit similar trends in the variation of $D_{Na}$ values with the change of electrode potential. They exhibit the minimum $D_{Na}$ values in the plateau region, whereas much higher values are obtain before and after the plateau. Similar phenomenon has also been detected in other electrode materials with two-phase mechanism such as $LiFePO_4$ and $Li_3V_2(PO_4)_3$ in previous reports[37,38]. It can be attributed to the strong interactions between the intercalation ions and the host matrix during two-phase transition reaction[37,38]. Although the carbon-coated reference sample ($10^{-12.7}$~$10^{-15.1}$ $cm^2$ $s^{-1}$) exhibits slightly increased $D_{Na}$ values than the low carbon-content reference sample ($10^{-13}$~$10^{-15.5}$ $cm^2$ $s^{-1}$), both references samples display much lower $D_{Na}$ values than the honeycomb-structured microball ($10^{-12}$~$10^{-14.5}$ $cm^2$ $s^{-1}$). Because the carbon-coated reference sample and the honeycomb-structured sample have similar carbon content, the superior sodium diffusion capability for the honeycomb-structured sample is mainly attributed to its hierarchical porous architecture.

EIS spectra of both samples are displayed in Figure 5 (b). Each Nyquist plot consists of a depressed semicircle and a sloping line. The depressed semicircle and the sloping line can be attributed to the charge transfer process and the solid-state diffusion of sodium ion, respectively[39,40]. Thus the charge transfer resistance ($R_{ct}$) can be estimated from the diameter of the high-frequency depressed semicircle. As compared in Figure 5(c), the carbon-coated reference sample exhibits slightly lower $R_{ct}$ value than the low carbon-content reference one. However, the $R_{ct}$ values of both reference samples are much higher than the honeycomb-structured microball. The results demonstrate the porous architecture is the major factor to suppress the charge transfer resistance and improve the sodium transfer capability for the honeycomb-structured sample. They are agreed with the GITT evaluation results.

Based on above discussion, the higher sodium diffusion capability of honeycomb-structured microballs is associated with its special hierarchical porous architecture. As schemed in Figure 5(e), the honeycomb-structure not only ensures high-efficient ion transport by improved electrolyte penetration, but also provides continuous electron transport pathways through constructing 3D conductive network. Both factors facilitate fast electron/ion transport chemistry and result in improved electrochemical property for the composite. Therefore, both EIS and GITT results confirm that the hierarchical porous honeycomb-type structure is highly efficient in modifying the ion intercalation kinetics for the polyanion-based materials. Furthermore, the larger difference between the honeycomb-structured microball and the carbon-coated reference sample also demonstrates the hierarchical porous architecture plays a more important role in the electrochemical kinetic improvement.

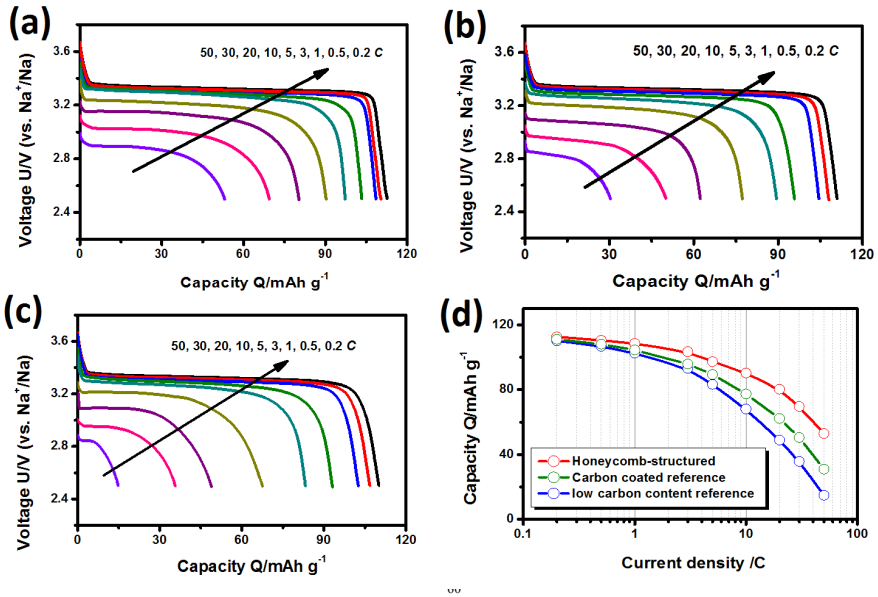


Figure 6 Galvanostatic discharge curves of the honeycomb-structured microball (a), carbon-coated reference sample (b) and low carbon-content reference sample (c) at different current densities. (d) Comparison of discharge capacities of all the materials under different current densities.

Inspired by the advantages of honeycomb-type architecture, the electrochemical behaviors of all the samples are investigated. First of all, the galvanostatic charge-discharge characteristics of all the samples under different current rates (i.e. 0.2, 0.5, 1, 3, 5, 10, 30 and 50 *C*) are investigated. For each sample, the discharge capacity decrease as current density increases (Figure 6a~d). When the current density is as low as 0.2 *C*, all the samples exhibits similar capacities. However, as the current is higher than 1 *C*, obviously higher capacities are observed for the honeycomb-structured microball in comparison to both reference samples. Meanwhile, the carbon-coated reference sample exhibits higher capacity than the low carbon-content reference one. As the current density increases, the difference between the samples becomes more significant. Especially, at the 5 *C* and 20 *C* rates, the capacities of 97.2 and 80.2 mAh·g$^{-1}$, corresponding to 86% and 71% of capacity at 0.2 *C*, are realized for the honeycomb-structured composite, which is much higher than the carbon-coated reference sample (89.3 and 62.2 mAh·g$^{-1}$) and low carbon-content reference sample (83.2 and 48.9 mAh·g$^{-1}$). The superior high rate capability of honeycomb-structured microball is associated with its unique hierarchical porous architecture and 3D conductive framework. It provides continuous electron pathways and high-efficient ion pathways, which results in the improved electrochemical kinetics intrinsically and is favorable to fast ion intercalation chemistry. Moreover, the large difference between the honeycomb-structured microball and the carbon-coated reference sample further demonstrates that the hierarchical porous architecture plays a more important role on the high rate capability. They are coincided with sodium diffusion capability evaluation results in above the GITT and EIS measurements.

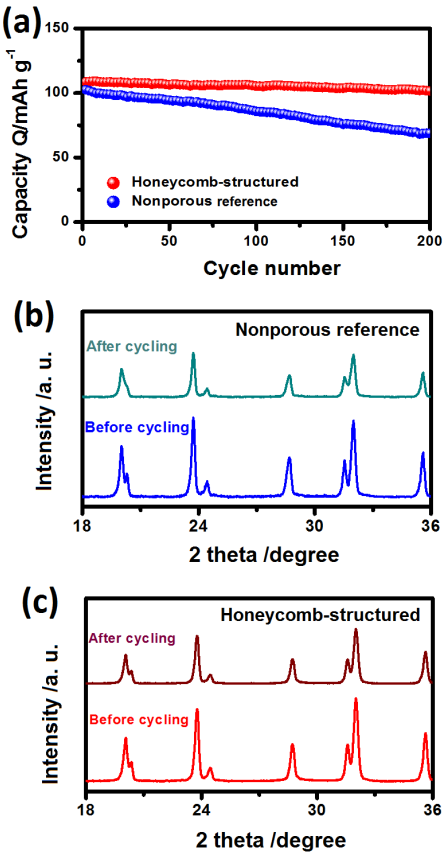


Figure 7 (a) Cycling performance of the honeycomb-structured microball and low carbon-content reference sample at the 1 *C* rate. Comparison of the *ex-situ* XRD patterns of the low carbon-content reference electrode (b) and honeycomb-structured (c) electrode before and after 200 cycles.

The long-term cycling performance of the honeycomb-structured and low carbon-content reference samples is evaluated at two current densities of 1 *C* and 20 *C*. As displayed in Figure 7(a) and S3, the capacity retentions of honeycomb-structured composite are respectively 93.6% and 81.9% at 1 *C* and 20 *C* after cycles, which are much higher than those of the low carbon-content reference sample (67.1% at 1 *C* and 29.9% at 20 *C*). The *ex-situ* XRD patterns of the cycled electrodes are collected. As shown in Figure 7(b, c), obvious peaks weaken and broaden are observed in the XRD patterns of both cycled electrodes in comparison to those of the original ones, indicating the structure deterioration upon cycling. Compared with the low carbon-content reference sample, much higher peak intensities are observed for the honeycomb-structured sample after the same cycling. The slower structure deterioration rate of the honeycomb-structured sample upon cycling is associated with its hierarchical porous structure and surface carbon layer. It acts as a buffer layer that alleviates volume change during ion insertion/extraction and results in improved structure stability and cycling property. This advantage has also been observed in other hierarchical porous electrode materials as cycled in "rocking-chair" systems[17-19,21,35]. On the basis of all above results, it certifies that the honeycomb-type architecture is favorable to realizing superb high rate capability and cycling stability for the polyanion-based materials, which puts forwards a promising strategy to modify the electrode materials in sodium ion batteries.

## 4 Conclusions

In summary, a new structured material, named "honeycomb-type hierarchical porous microball" has been designed and fabricated to develop high-performance polyanion-based electrode materials. The honeycomb-type structure is composed of hierarchical pores and possesses a lot of interconnective nanochannels, which effectively improves the electrolyte penetration and constructs high-efficient ion transport pathway. The network between hierarchical pores consists of single crystal skeleton and *in-situ* carbon surface layer. It constructs a 3D conductive framework inside the microballs and acts as a buffer for volume change during ion insertion/extraction. As a case study, the honeycomb-structured $Na_3V_2(PO_4)_3$/C microballs are employed as the first target material via a one-pot synthesis. It exhibits superior high rate capability and cycling stability than the microsized nonporous reference sample. The improved properties can be attributed to the synergistic effects of hierarchical porous nanostructure and 3D continuous conductive framework. Both factors provide effective electron/ion pathways for fast kinetic and result in superior crystal stability upon cycling. Therefore, the honeycomb-type structure is demonstrated to be a promising strategy for polyanion materials, in view of wide validity, superior property and easy production.

## Acknowledgements

This work is supported by the National Natural Science Foundation of China (No. 21001036, 50902041), Program for New Century Excellent Talents in Heilongjiang Provincial University (1253-NCET-012), Natural Science Foundation of Heilongjiang Province (No. QC2013C008) and Heilongjiang Teaching Reform Project of Academic Degree and Postgraduate Education (No. JGXM-HLJ-2014024).

## Notes and references

[a]*Key Laboratory for Photonic and Electronic Bandgap Materials, Ministry of Education; College of Chemistry and Chemical Engineering, Harbin Normal University, Harbin, 150025, Heilongjiang, China; E-Mail: chaodenghsd@sina.com*

[b]*Key Laboratory of Superlight Material and Surface Technology, Ministry of Education, College of Material Science and Chemical Engineering, Harbin Engineering University, Harbin 150001, Heilongjiang, China; E-Mail: senzhang@hrbeu.edu.cn*

[c]*Northeast Agricultural University, Harbin, 150030, Heilongjiang, China*

‡ Both authors contribute equally to this article.

†Electronic Supplementary Information (ESI) available: Morphology, atomic parameters and lattice parameters of the carbon-coated reference sample and low carbon-content reference sample, relationship between the transient voltage ($E$) and square root of $\tau$ in a titration process, cycling property of the honeycomb-structured microball and low carbon-content reference sample at the 20 *C* rate. See DOI: 10.1039/b000000x/

1 J. M. Tarascon, M. Armand, *Nature* **2001**, *4*, 359-367.
2 M. S. Whittingham, *Chem. Rev.* **2004**, *104*, 4271-4302.
3 A. Yamada, N. Iwane, Y. Harada, S. Nishimura, Y. Koyama, I. Tanaka, *Adv. Mater.* **2010**, *22*, 3583-3587.
4 K. Amine, R. Kanno, Y. Tzeng, *MRS Bull.* **2014**, *39*, 395-401.
5 L. Tan, S. Zhang, C. Deng, *J. Power Sources* **2015**, *275*, 6-13.
6 V. Palomares, P. Serras, I. Villaluenga, K. B. Hueso, J. C. Gonzalez, T. Rojo, *Energy Environ. Sci.* **2012**, *5*, 5884-5901.
7 P. Barpanda, G. Oyama, S. I. Nishimura, S. C. Chung, A. Yamada, *Nat. Commu.* **2014**, *5*, 4358.
8 N. Yabuuchi, K. Kubota, M. Dahbi, S. Komaba, *Chem. Rev.* **2014**, *114*, 11636-11682.
9 S. Zhang, C. Deng, Y. Meng, *J. Mater. Chem. A* **2014**, *2*, 20538-20544.
10 C. Deng, S. Zhang, L. Ma, Y. H. Sun, S. Y. Yang, B. L. Fu, F. L. Liu, Q. Wu, *J. Alloys Compd.* **2011**, *509*, 1322-1327.
11 C. Deng, S. Zhang, Z. Dong, Y. Shang, *Nano Energy* **2014**, *4*, 49-55.
12 D. Han, S. Lim, Y. Kim, S. Kang, Y. Lee, Y. Kang, *Chem. Mater.* **2014**, *26*, 3644-3650.
13 X. Lu, Y. Shang, S. Zhang, C. Deng, *Electrochim. Acta* **2015**, *155*, 148-156.
14 D. Tu, B. Wu, B. Wang, C. Deng, Y. Gao, *Appl. Catal. B Environ.* **2011**, *103*, 163-168.
15 S. Li, Y. Dong, L. Xu, X. Xu, L. He, L. Mai, *Adv. Mater.* **2014**, *26*, 3545-3553.
16 S. Kim, H. Jeong, J. Kwon, I. Ock, W. Suh, G. Stucky, J. Kang, *Energy Environ. Sci.* **2015**, *8*, 188-194.
17 Y. Ko, S. Park, K. Jung, Y. Kang, *Nano Lett.* **2014**, *13*, 5462-5466.
18 J. Jin, S. Huang, J. Liu, Y. Li, D. Chen, H. Wang, H. Yu, L. Chen, B. Su, *J. Mater. Chem. A* **2014**, *2*, 9699-9708.
19 C. Zhang, Z. Chen, Z. Guo, X. Lou, *Energy Environ. Sci.* **2013, 6,** 974-978.
20 A. Pan, H. Wu, L. Yu, X. Lou, *Angew. Chem.* **2013**, *125*, 2282-2286.

21 Y. Xia, Z. Xiao, H. Huang, X. Lu, R. Yan, Y. Gan, W. Zhu, J. Tu, W. Zhang, X. Tang, *ACS Nano* **2013**, *7*, 7083-7092.

22 D. Jung, H. Hwang, J. Lee, H. Koo, R. Shakoor, R. Kahraman, Y. Jo, M. Park, J. Choi, *Nano Lett.* **2014**, *14*, 4418-4425.

23 B. Choi, M. Yang, W. Hong, J. Choi, Y. Huh, *ACS Nano* **2012**, *6*, 4020-4028.

24 S. Dutta, A. Bhaumik, K. Wu, *Energy Enviorn. Sci*. **2014**, *7*, 3574-3592.

25 D. Piper, J. Woo, S. Son, S. Kim, K. Oh, S. Lee, *Adv. Mater.* **2014**, *26*, 3520-3525.

26 Y. Wang, Q. Zhu, H. Zhang, *J. Mater. Chem.* **2006**, *16*, 1212-1214.

27 Y. Shin, J. Liu, L. Wang, Z. Nie, W. Samuels, G. Fryxell, G. Exarhos, *Angew. Chem.* **2000**, *112*, 2814-2819.

28 P. Nie, Y. Zhu, L. Shen, G. Pang, G. Xu, S. Dong, H. Dou, X. Zhang, *J. Mater. Chem. A* **2014**, *2*, 18606-18612.

29 S. Lim, D. Han, D. Nam, K. Hong, J. Eom, W. Ryu, H. Kwon, *J. Mater. Chem. A* **2014**, *2*, 19623-19632.

30 J. Yang, D. Hang, M. Jo, K. Song, Y. Kim, S. Chou, H. Liu, Y. Kang, *J. Mater. Chem. A* **2015**, *3*, 1005-1009.

31 C. Zhu, K. Song, P. Aken, J. Maier, Y. Yu, *Nano Lett.* **2014**, *14*, 2175-2180.

32 W. X. Song, X. B. Ji, Y. P. Yao, H. J. Zhu, Q. Y. Chen, Q. Q. Sun, C. E. Banks, *Phys. Chem. Chem. Phys.* **2014**, *16*, 3055-3061.

33 Y. Meng, S. Zhang, C. Deng, *J. Mater. Chem. A* **2015**, 3, 4484-4492.

34 A. Ferrari, J. Robertson, *Phys. Rev. B* **2000**, *61*, 14095-14107.

35 J. Jin, S. Huang, J. Liu, Y. Li, D. Chen, H. Wang, Y. Yu, L. Chen, B. Su, *J. Mater. Chem. A* **2014**, *2*, 9699-9708.

36 L. Tan, S. Zhang, C. Deng, *J. Power Sources* **2015**, *275*, 6-13.

37 K. Tang, X. Yu, J. Sun, H. Li, X. Huang, *Electrochim. Acta* **2011**, *56*, 4869-4875.

38 X. Rui, N. Ding, J. Liu, C. Li, C. Chen, *Electrochim. Acta* **2010**, *55*, 2384-2390.

39 S. Zhang, C. Deng, S. Y. Yang, H. Niu, *J. Alloys Compd.* 2009, *484*, 519-523.

40 P. Liu, J. Vajo, J. Wang, W. Li, J. Liu, *J. Phys. Chem. C* **2012**, *116*, 6467-6473.